Cell Reports

A Role for FACT in RNA Polymerase II Promoter-Proximal Pausing

Graphical Abstract

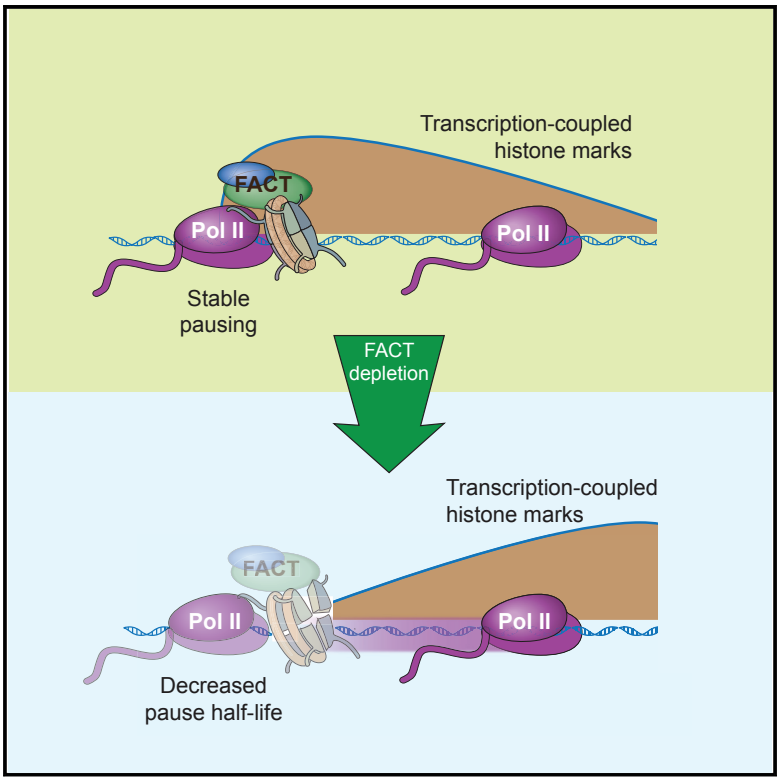

Highlights

- FACT regulates patterns of transcription-coupled histone marks
- FACT knockdown reduces the half-life of promoter-proximally paused Pol II
- FACT helps to maintain promoter-proximal Pol II pausing

Authors

Theophilus T. Tettey, Xin Gao, Wanqing Shao, ..., Julia Zeitlinger, Marco Blanchette, Joan W. Conaway

Correspondence

jlc@stowers.org

In Brief

FACT is a histone chaperone implicated in the assembly and disassembly of nucleosomes during transcription. Tettey et al. demonstrate that *Drosophila* FACT regulates patterns of the transcription-coupled histone marks H3K4me3 and H3K36me3 and helps to maintain promoter-proximal Pol II pausing.

Tettey et al., 2019, Cell Reports *27*, 3770–3779
June 25, 2019
https://doi.org/10.1016/j.celrep.2019.05.099

CellPress

OPEN ACCESS
CellPress

Cell Reports
Report

A Role for FACT in RNA Polymerase II Promoter-Proximal Pausing

Theophilus T. Tettey,[1,2] Xin Gao,[1,6] Wanqing Shao,[1] Hua Li,[1] Benjamin A. Story,[1,7] Alex D. Chitsazan,[1,8] Robert L. Glaser,[3] Zach H. Goode,[1] Christopher W. Seidel,[1] Ronald C. Conaway,[1,4] Julia Zeitlinger,[1,5] Marco Blanchette,[1,9] and Joan W. Conaway[1,4,10,*]

[1]Stowers Institute for Medical Research, 1000 E 50th St, Kansas City, MO 64110, USA
[2]The Open University, Walton Hall, Milton Keynes, Buckinghamshire MK7 6AA, UK
[3]Wadsworth Center, New York State Department of Health, PO Box 509, Albany, NY 12201, USA
[4]Department of Biochemistry and Molecular Biology, University of Kansas Medical Center, Kansas City, KS 66160, USA
[5]Department of Pathology and Laboratory Medicine, University of Kansas Medical Center, Kansas City, KS 66160, USA
[6]Present address: State Key Laboratory of Experimental Hematology, Institute of Hematology & Blood Disease Hospital, Center for Stem Cell Medicine, Chinese Academy of Sciences & Peking Union Medical College, Tianjin, China
[7]Present address: EMBL Heidelberg, Meyerhofstrasse 1, 69117 Heidelberg, Germany
[8]Present address: OHSU Knight Cancer Center CEDAR, 2720 SW Moody Avenue, Portland, OR 97201, USA
[9]Present address: Dovetail Genomics, Santa Cruz, CA 95060, USA
[10]Lead Contact
*Correspondence: jlc@stowers.org
https://doi.org/10.1016/j.celrep.2019.05.099

SUMMARY

FACT (facilitates chromatin transcription) is an evolutionarily conserved histone chaperone that was initially identified as an activity capable of promoting RNA polymerase II (Pol II) transcription through nucleosomes *in vitro*. In this report, we describe a global analysis of FACT function in Pol II transcription in *Drosophila*. We present evidence that loss of FACT has a dramatic impact on Pol II elongation-coupled processes including histone H3 lysine 4 (H3K4) and H3K36 methylation, consistent with a role for FACT in coordinating histone modification and chromatin architecture during Pol II transcription. Importantly, we identify a role for FACT in the maintenance of promoter-proximal Pol II pausing, a key step in transcription activation in higher eukaryotes. These findings bring to light a broader role for FACT in the regulation of Pol II transcription.

INTRODUCTION

FACT (facilitates chromatin transcription) was originally identified in human cell extracts as an activity capable of promoting RNA polymerase II (Pol II) transcription through nucleosomes (Orphanides et al., 1998). FACT is an evolutionarily conserved, heterodimeric protein (Formosa, 2008; Orphanides et al., 1999). It functions much like a histone chaperone to promote Pol II transcription of chromatin *in vitro*, by aiding in the disassembly and reassembly of nucleosomes encountered by transcribing polymerase (Belotserkovskaya et al., 2003). Subsequent genetic studies defined a broader role for FACT in maintaining chromatin architecture. Loss of FACT function can lead to a variety of chromatin abnormalities, including (1) loss or disorganization of nucleosomes and mislocalization of the yeast histone H2A.Z in transcribed regions (Feng et al., 2016; Jamai et al., 2009; Jeronimo et al., 2015; Schwabish and Struhl, 2004; Voth et al., 2014; Xin et al., 2009); (2) reduced levels of bulk trimethylation of histone H3 at lysine 36 (H3K36me3) in yeast (Chu et al., 2006); and (3) aberrant transcription-coupled histone H3 lysine 4 trimethylation (H3K4me3) at immunoglobulin switch regions (Stanlie et al., 2010). Notably, mammalian FACT is most highly expressed in undifferentiated and stem-like cells. Elevated expression of the FACT subunit SSRP1 is associated with poor clinical outcome in many cancers, and interfering with FACT activity has been reported to block growth of tumor cells *in vitro* and *in vivo* (Carter et al., 2015; Dermawan et al., 2016; Ding et al., 2016; Garcia et al., 2011, 2013; Gasparian et al., 2011; Hossan et al., 2016).

Although FACT was originally identified in human cells, its function is best understood in yeast. To shed light on the function(s) of FACT in higher eukaryotes, we investigated the consequences of decreasing FACT expression in *Drosophila* S2 cells. We observe that decreased FACT expression leads to a dramatic redistribution of the transcription-associated histone marks H3K4me3 and H3K36me3. Most notably, we identify a role for FACT in maintaining promoter-proximal Pol II pausing, a process that is apparently absent from budding yeast but plays an important role in transcription activation at most higher eukaryotic genes (Jonkers and Lis, 2015; Liu et al., 2015). Promoter-proximal pausing occurs when Pol II initiates transcription at a promoter, synthesizes a short transcript of ~20–60 nucleotides, and then enters a paused state until it either terminates (Brannan and Bentley, 2012; Brannan et al., 2012; Wagschal et al., 2012) or is released into productive elongation. Release from promoter-proximal pausing is a key step in gene activation in response to many signaling pathways. Our identification of a role for FACT in Pol II promoter-proximal pausing expands the function of FACT in transcription.

RESULTS

FACT Enrichment in Gene 5′ Ends

Results of previous studies led to the model that FACT promotes Pol II transcription by traveling with elongating Pol II.

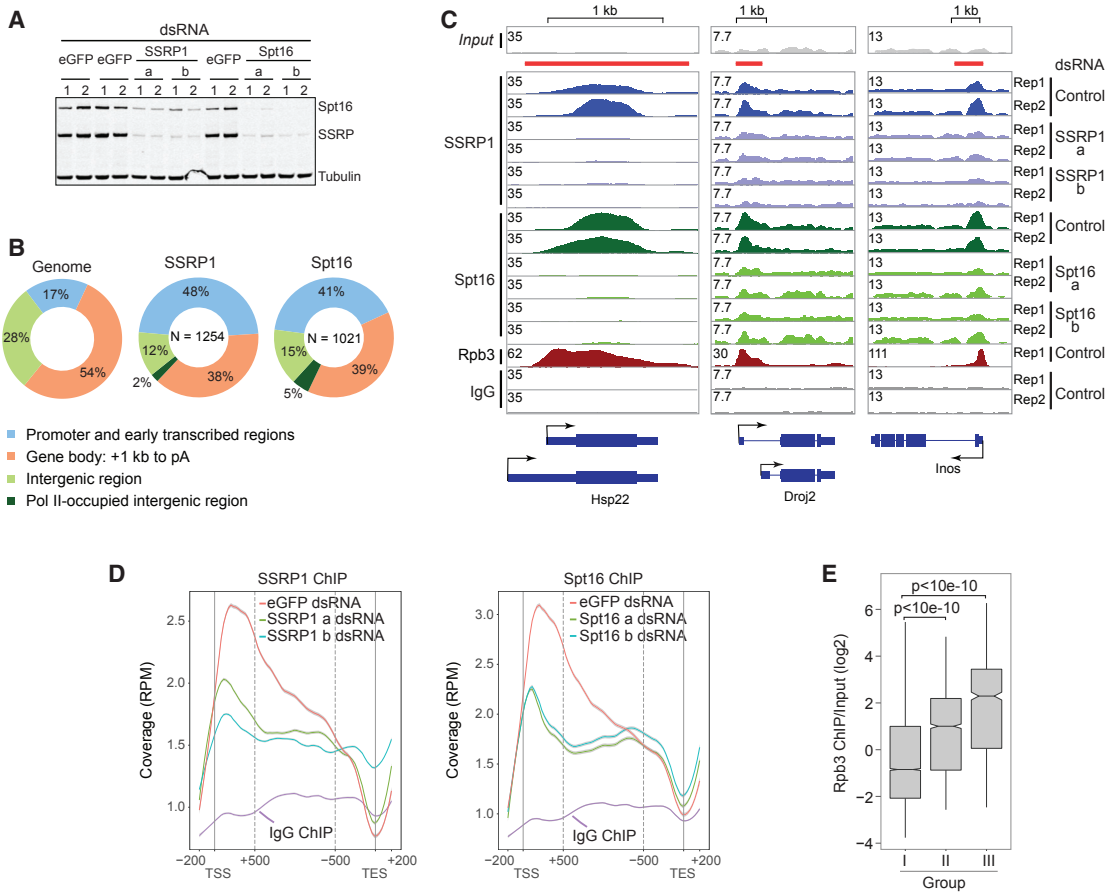

Figure 1. FACT Is Enriched in the Promoter and Early Transcribed Regions of Pol II-Occupied Genes

(A) Western blot of Spt16 and SSRP1 in *Drosophila* S2 cells treated with EGFP, SSRP1, and Spt16 double-stranded RNAs (dsRNAs). Tubulin was used as a loading control.

(B) Pie chart showing enrichment in gene 5′ ends of high-confidence FACT peaks (MACS2 fold change [FC] > 1.5 over knockdown, FDR $\leq 10^{-2}$). N, total number of SSRP1 or Spt16 peaks; promoter and early transcribed regions, −200 bp to +1,000 bp relative to TSS; gene body (+1,000 bp to the polyadenylation site); intergenic region (peaks between genes).

(C) Integrated genome viewer (IGV) browser track examples of SSRP1 (blue), Spt16 (green), and Rpb3 (red) ChIP-seq signals at three group III genes from S2 cells treated with EGFP, SSRP1, and Spt16 dsRNAs. Rep1, replica 1; Rep2, replica 2. The red horizontal bars indicate positions of FACT peaks identified by MACS2.

(D) Metagene plots showing SSRP1 and Spt16 ChIP signals at 876 genes that are longer than 1.5 kb and have high-confidence SSRP1 or Spt16 peaks in cells treated with EGFP, SSRP1, or Spt16 dsRNAs.

(E) Boxplot showing correlation of Pol II enrichment with FACT occupancy in promoters and early transcribed regions. p values were calculated using Wilcoxon rank sum test of pairwise comparisons.

Also see Figure S1.

FACT co-localizes closely with transcribing Pol II in yeast (Mason and Struhl, 2003) and on *Drosophila* polytene chromosomes (Saunders et al., 2003). To explore further the relationship of FACT and Pol II in *Drosophila* S2 cells, we compared their localizations in chromatin immunoprecipitation sequencing (ChIP-seq) experiments.

To localize FACT, we performed ChIP-seq using antibodies against *Drosophila* FACT subunits SSRP1 and Spt16. The peak finding algorithm MACS2 was used to identify loci occupied by SSRP1 or Spt16, using as controls SSRP1 or Spt16 ChIP-seq datasets from cells depleted of SSRP1 or Spt16, respectively. SSRP1 or Spt16 was each depleted using two non-overlapping double-stranded RNAs (dsRNAs); EGFP double-stranded RNA was used as a non-targeting control. After knockdown of either FACT subunit, expression of SSRP1 and Spt16 was reduced to about 20%–30% of that seen in cells treated with EGFP dsRNA (Figure 1A). Knocking down SSRP1 or Spt16 reduced the expression of both proteins, consistent with prior evidence that depletion of one FACT subunit leads to reduced stability of the other in human cells (Safina et al., 2013). Examples of FACT-occupied regions in control and SSRP1- or Spt16-knockdown cells are shown in Figure 1C.

The *D. melanogaster* genome was partitioned into promoter and early transcribed region (200 bp upstream to 1 kb downstream of the transcription start site [TSS]), gene body (+1 kb to polyadenylation site), and intergenic regions lacking

annotated transcripts. We observed that 86% of the SSRP1 peaks and 80% of the Spt16 peaks (MACS2, fold change > 1.5 over knockdown, false discovery rate [FDR] $\leq 10^{-2}$) fell within promoter and transcribed regions of annotated genes, with a bias toward the 5′ ends (Figure 1B). Regions exhibiting the highest SSRP1 and Spt16 enrichment were dominated by stress response genes, including *Hsp22*, *Hsp23*, *Hsp26*, *Hsp27*, and *Hsp70*, consistent with previous evidence for high FACT occupancy at heat shock genes (Saunders et al., 2003). SSRP1 and Spt16 occupancy was highly correlated as expected since they function together as subunits of the heterodimeric FACT complex (Figure S1B).

We also performed a ChIP of total Pol II using an antibody targeting the Pol II subunit Rpb3. Regions of highest FACT enrichment peaked within the first few hundred base pairs downstream of the TSS, downstream of promoter-proximally paused Pol II (Figures 1D and S1C). We then compared Rpb3 enrichment in the 5′ end of genes (200 bp upstream to 1 kb downstream of the TSS). Genes without detectable FACT enrichment (group I, n = 13,313) had lower Pol II occupancy, while the 1,015 genes with the greatest FACT enrichment (MACS2 fold change > 1.5 and FDR $\leq 10^{-2}$; group III) exhibited the highest Pol II occupancy (Figure 1E). An additional 2,683 genes with lower confidence FACT peaks (group II, FDR $\leq 10^{-1}$, excluding group III genes) also showed increased Pol II occupancy relative to group I genes. Thus, FACT is most highly enriched at genes with higher levels of Pol II. In addition, we note that Pol II overlaps with a fraction of the FACT peaks that mapped to intergenic regions, as exemplified in the browser shots shown in Figure S1A. However, not all genes containing discernable Pol II have detectable FACT peaks, suggesting either that FACT is only present at a subset of Pol II transcribed genes or, perhaps more likely, that our antibodies are not sensitive enough to detect FACT at loci with relatively low levels of Pol II.

FACT Knockdown Alters Global Patterns of Transcription-Coupled Histone Marks

The N-terminal tails of histones are subject to extensive post-translational modifications. Among these are H3K4me3 and H3K36me3, both of which are closely linked to transcription. H3K4 trimethylation by a complex of proteins associated with Set1 (COMPASS)-like histone methyltransferases is targeted to the 5′ ends of genes via Pol II that has been phosphorylated on Ser5 of its carboxy-terminal domain (CTD) during or shortly after initiation, while H3K36me3 by Set2 is targeted to gene bodies through interaction with elongating Pol II phosphorylated on Ser2 of its CTD by the pause-release kinase positive transcription elongation factor b (P-TEFb) (Shilatifard, 2012; Venkatesh and Workman, 2013; Woo et al., 2017).

Previous studies have linked FACT to both of these transcription-coupled histone modifications. Loss of FACT in a mouse B cell lymphoma cell line leads to loss of H3K4me3 in Sμ and Sα immunoglobulin class switch regions and interferes with transcription-dependent class switch recombination (Stanlie et al., 2010). In addition, levels of bulk H3K36me3 were shown to be reduced in a yeast *spt16* mutant (Chu et al., 2006); however, the genomic distribution of the H3K36me3 mark was not examined in this study.

For these reasons and because of FACT's enrichment at transcriptionally active loci, we wished to explore the consequences of FACT depletion on the distribution of transcription-associated histone modifications. To do so, we treated S2 cells with control EGFP dsRNA or dsRNAs targeting SSRP1 or Spt16 and performed H3K4me3 and H3K36me3 ChIP-seq. Because our FACT knockdowns only partially deplete FACT subunits, it is likely that our experiments will only reveal consequences of FACT depletion in processes that are most sensitive to FACT concentration. In addition, because it takes several days to achieve dsRNA-mediated knockdown of SSRP1 and Spt16, some phenotypes associated with FACT depletion could be indirect.

Average gene plots were generated for transcribed genes that are longer than 1.5 kb and, to reduce signals associated with overlapping or nearby genes, are separated from all other genes by at least 200 bp. As expected, control cells showed a strong enrichment of H3K4me3 at gene 5′ ends as observed in average gene plots (Figure 2A) and at individual genes, exemplified in Figure 2B by *Inos* and *18w*. After SSRP1 or Spt16 knockdown, H3K4me3 signals were broadened, with reduced H3K4me3 in gene 5′ ends and a modest increase in H3K4me3 across transcribed regions. The effect of FACT depletion on H3K4me3 was evident on the majority of transcribed genes included in our analysis, including group I, II, and III genes (Figure 2C).

H3K36me3 distribution was also aberrant after FACT knockdown (Figures 2D and 2E). H3K36me3 was reduced across a large portion of transcription units but showed little or no change in the last few hundred bp before polyadenylation sites, resulting in an overall 5′ to 3′ shift in the distribution of this mark. As with H3K4me3, the effect of FACT depletion on H3K36me3 was broadly distributed (Figure 2F).

In yeast *spt16* mutants, substantial transcription-dependent nucleosome loss was detected by ChIP of core histones, including H3, within the transcribed regions of genes (Jamai et al., 2009; Jeronimo et al., 2015; Schwabish and Struhl, 2004; Voth et al., 2014; Xin et al., 2009). To address the possibility that changes in H3K4me3 and H3K36me3 marks could be explained by changes in histone H3 occupancy rather than changes in the distribution of these histone modifications per se, we performed a histone H3 ChIP-seq experiment. Average gene plots of H3 occupancy (Figure 2G) revealed only subtle changes in histone H3 distribution and perhaps a slight decrease in average H3 occupancy over the bodies of transcribed genes after either SSRP1 or Spt16 knockdown. The differences, if any, in H3 occupancy within the first 500 bp or throughout the entire gene body were much less than those observed for the H3K4me3 and H3K36me3 marks, respectively (Figures 2C and 2F). We also investigated the effect of FACT knockdown on histone H3 occupancy at several FACT-occupied group III genes using ChIP-qPCR (Figure S2). These assays showed little or no difference in H3 occupancy at either the promoter or gene body regions of the genes analyzed. The apparent difference between the effects of mutating Spt16 in yeast and knocking down Spt16 or SSRP1 in *Drosophila* S2 cells may be because (1) FACT is only partially depleted after dsRNA-mediated knockdown and (2) the residual FACT is sufficient for all but the most sensitive FACT-dependent effects. Alternatively, FACT-dependent

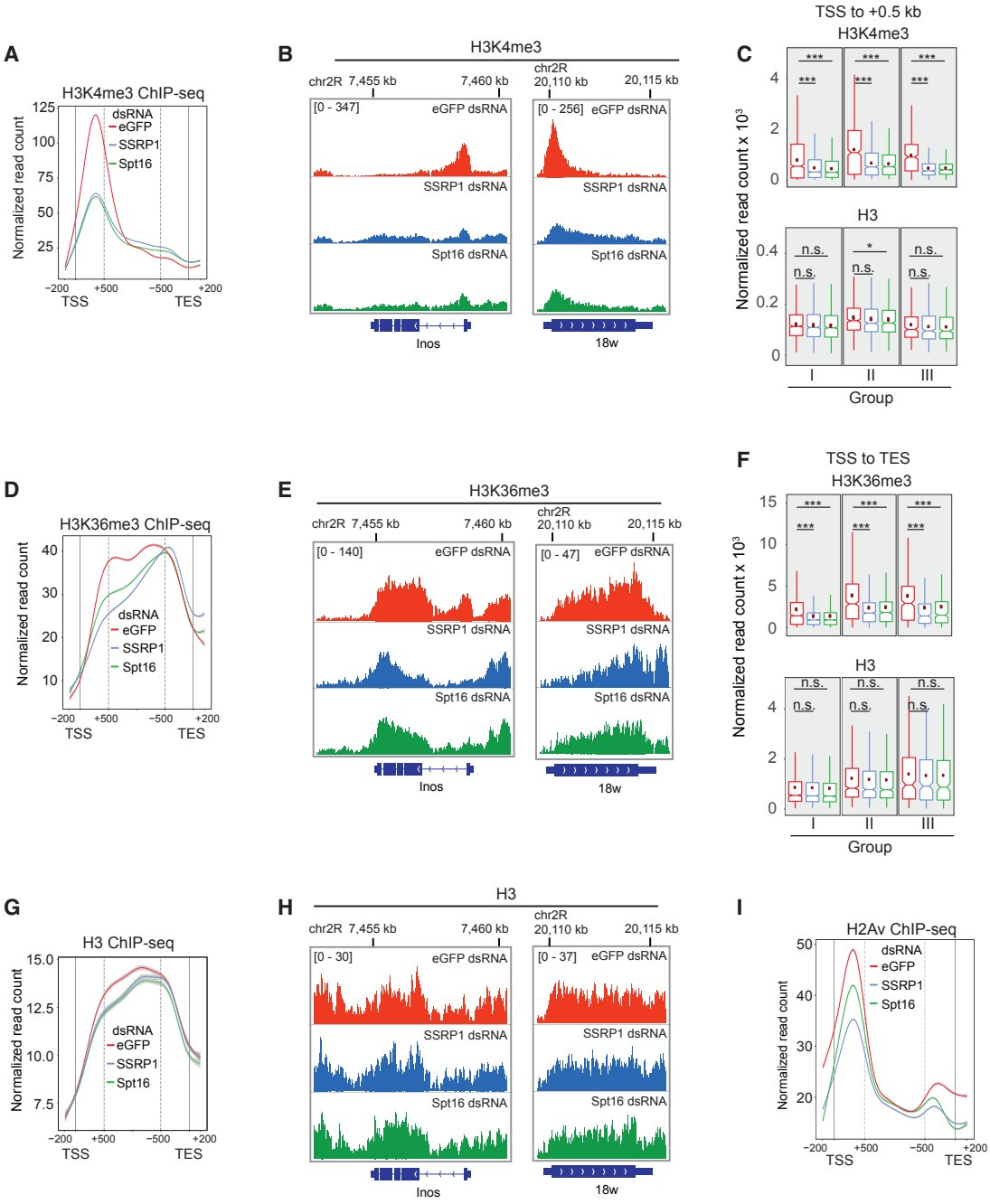

Figure 2. Effect of FACT Depletion on Histone Occupancy and Transcription-Associated Histone Marks

(A, D, G, and I) Average H3K4me3 (A), H3K36me3 (D), H3 (G), and H2Av (I) enrichment over 1,556 non-overlapping active genes that are longer than 1.5 kb and have no neighboring genes within 200 bp in S2 cells treated with EGFP, SSRP1, or Spt16 dsRNAs. Shaded areas in this and all other metaplots represent 95% confidence interval predicted from a generalized additive model.

(B, E, and H) IGV genome browser tracks showing H3K4me3 (B), H3K36me3 (E), and H3 (H) ChIPs.

(C) Normalized read counts of H3K4me3 and H3 signals from TSS to +500 bp at groups I (n = 1,137), II (n = 565), and III (n = 321) genes longer than 1 kb with no neighboring genes within 200 bp following treatment with EGFP (red), SSRP1 (blue) and Spt16 (green) dsRNA.

(F) Normalized read counts of H3K36me3 and H3 signals from TSS to TES at group I, II, and III genes following treatment with EGFP (red), SSRP1 (blue), and Spt16 (green) dsRNA.

p values in (C) and (F) were calculated using Wilcoxon rank sum test of pairwise comparisons. Here and in subsequent figures, red dots show average values. *$p \leq 0.05$; **$p \leq 0.01$; ***$p \leq 0.001$; n.s., not significant. Also see Figures S2 and S3.

changes in nucleosome occupancy could be obscured by compensatory mechanisms in S2 cells. Regardless of why FACT knockdown has only minimal effects on H3 occupancy in S2 cells, these observations argue that changes in the distribution of H3K4me3 and H3K36me3 cannot be explained by changes in H3 distribution. Thus, our findings support the model that FACT is needed for proper localization of transcription-associated chromatin marks in *Drosophila*.

We also investigated the effect of depleting FACT on the distribution of the histone H2A variant H2A.Z in *Drosophila* S2 cells. Recent studies have implicated yeast FACT in restricting H2A.Z to promoter regions (Jeronimo et al., 2015). Loss of yeast FACT leads to a loss of H2A.Z from promoter-proximal nucleosomes coupled with an increase in H2A.Z in gene bodies. These changes were attributed to mislocalization of SWR complex (SWR-C), which is responsible for the exchange of H2A.Z/H2B dimers into nucleosomes. To determine whether depletion of *Drosophila* FACT also leads to changes in H2A.Z localization, we compared the occupancy of H2Av (the *Drosophila* ortholog of H2A.Z) before and after FACT knockdown. As expected (Bruce et al., 2005; Guillemette et al., 2005; Raisner et al., 2005; Zhang et al., 2005), H2A.v marks the 5′ ends of genes in both control cells and cells depleted of FACT subunits (Figure 2I). Consistent with evidence that FACT is needed to retain H2A.v at promoter regions in yeast (Jeronimo et al., 2015), we observed a widespread reduction of H2A.v at gene 5′ ends after FACT knockdown (Figures 2I and S3A). We also observed an increase in H2A.v in the bodies of some genes (Figure S3B); however, these changes were neither widespread nor evident in average gene plots. We note that we readily observed increases in H3K4me3 occupancy in gene bodies accompanying a decrease in promoter-proximal peaks. Hence, we expect that if there are widespread increases in H2Av occupancy in gene bodies after partial FACT depletion, they are less substantial than the H3K4me3 increases.

FACT Knockdown Leads to a Decrease in Promoter-Proximally Paused Pol II

We next explored the effect of FACT depletion on Pol II transcription in *Drosophila* cells. Previous studies have provided evidence that in yeast the loss of FACT can give rise to multiple transcription defects, including alterations in promoter usage and defective elongation (Biswas et al., 2005; Kaplan et al., 2003; Mason and Struhl, 2003; Schwabish and Struhl, 2004). Initially, we assessed the effect of FACT depletion on steady-state transcript levels using poly(A)-selected libraries from control or FACT-knockdown S2 cells, with human 293T cells as spike-in controls. Although we observed widespread changes in transcription-associated histone marks after FACT knockdown, changes in steady-state RNA levels were more limited; out of ~7,800 expressed genes we identified only 878 differentially expressed genes, about two-thirds of which were upregulated after SSRP1 or Spt16 knockdown (Figure S4A).

To investigate further the effect of FACT depletion on Pol II transcription, we used precision nuclear run-on coupled to deep sequencing (PRO-seq) (Kwak et al., 2013; Mahat et al., 2016) to measure Pol II occupancy genome wide in S2 cells treated with control and SSRP1 dsRNAs. We used PRO-seq rather than Pol II ChIP-seq for these experiments because (1) it generates strand-specific information, hence, one can distinguish between Pol II transcribing in the sense- and anti-sense direction on each gene, and (2) it measures only transcriptionally engaged polymerases.

Depletion of SSRP1 led to a widespread decrease in PRO-seq reads just downstream of the TSS, in the position of promoter-proximally paused Pol II, suggesting that FACT depletion decreases the amount of paused Pol II at many genes (Figure 3A). To explore the effect of FACT depletion on Pol II distribution further, we determined a pause index (PI), defined as the ratio of Pol II occupancy (based on PRO-seq reads) in the promoter-proximal region to Pol II occupancy in the gene body, a widely used metric to assess promoter-proximal Pol II pausing (Core et al., 2008; Muse et al., 2007; Zeitlinger et al., 2007). Based on their PIs, we subdivided our group of non-overlapping, transcribed genes into three equal groups (Figure 3B), designated highly paused, moderately paused, and lowly paused, and calculated the change in PI upon SSRP1 knockdown for all genes in each group. As shown in Figure 3C, loss of SSRP1 led to a decrease in PI at both highly and moderately paused genes; however, the effect was greatest at genes that are highly paused. Not surprisingly, there was little change in PI at lowly paused genes after SSRP1 knockdown.

Changes in PI can result from changes in the PRO-seq signal at the TSS, within the gene body, or both. In average gene plots of highly, moderately, and lowly paused genes, we observe little difference in PRO-seq reads in gene bodies, suggesting the majority of PI changes are due to changes in PRO-seq reads at the TSS region (Figure 3B). We also determined the change in PRO-seq reads over TSS and gene bodies in each pausing group. As shown in Figure S4B, the PRO-seq signal at the TSS is reduced at the majority of genes, and this reduction is most substantial at highly paused genes. On average, there are relatively small changes in the PRO-seq signal within gene bodies. However, the decrease in PRO-seq reads in the promoter-proximal region was associated with an increase in reads across the gene body in some cases, including *Hsp22*, *Hsp26*, and *18w* (Figures 3D, 3E, and S4B). As shown in Figure S4C, we found that genes that were upregulated in our RNA-seq dataset tended to exhibit this pattern, raising the possibility that in at least some cases the loss of FACT results in premature release of paused Pol II into productive elongation.

FACT Knockdown Leads to a Decrease in Pol II Pause Half-Life

A decrease in the amount of promoter-proximally paused Pol II can be due to a decrease in the duration of Pol II pausing, a decrease in initiation rate without a change in pause duration, or some combination of the two. To measure directly the effect of FACT depletion on the duration of promoter-proximal pausing, we used ChIP-nexus, a powerful method for high-resolution mapping of promoter-proximally paused Pol II using chromatin immunoprecipitation coupled to exonuclease footprinting (Shao and Zeitlinger, 2017).

In these experiments, we incubated cells that had been treated with EGFP control or SSRP1 dsRNAs with triptolide, a drug that blocks Pol II transcription initiation by inhibiting the

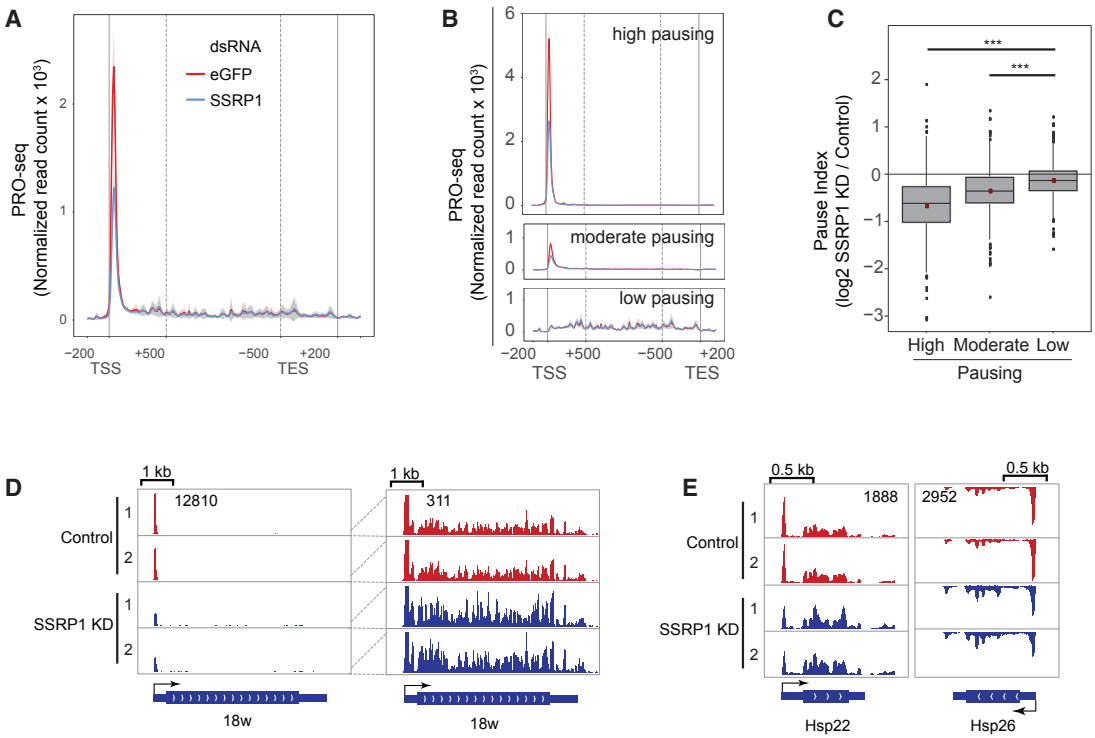

Figure 3. Altered Distribution of Transcriptionally Engaged Polymerase following FACT Depletion

(A) Average PRO-seq profile over transcribed regions in cells treated with EGFP or SSRP1 dsRNAs. Included in the profile are 1,556 non-overlapping, active genes that are longer than 1.5 kb and have no neighboring genes within 200 bp.

(B) Average PRO-seq coverage of highly, moderately, and lowly paused genes.

(C) PI change following SSRP1 knockdown across genes with varying degrees of pausing. p values were calculated using Wilcoxon rank sum test of pairwise comparisons.

(D and E) IGV genome browser tracks showing PRO-seq signals at *18w* (D), *Hsp22* (E), and *Hsp26* (E). In (D), panel on the right shows a rescaled version to emphasize changes in signal in the body of *18w*.

Also see Figure S4.

transcription factor IIH (TFIIH)-associated XPB helicase, but does not interfere with subsequent steps of transcription, including pause release (Jonkers et al., 2014; Titov et al., 2011; Vispé et al., 2009). Cells were harvested at various times after triptolide addition and subjected to Rpb3 ChIP-nexus; spike-in controls were included to account for the loss of total ChIP signal over time.

From the genes used above, we selected the 998 genes that had a promoter-proximal ChIP-nexus Pol II signal at an identifiable pausing position (Shao and Zeitlinger, 2017). For each of these genes, Pol II measurements from the time course were fitted into an exponential decay model (Figure 4A shows *18w* as an example). We observed a striking decrease in the half-life of paused Pol II at the majority of genes (Figures 4B) after SSRP1 depletion; this decrease was not limited to genes showing the greatest FACT enrichment (Figure S4D). A heatmap showing the promoter-proximal ChIP-nexus signal across all promoters, ranked by decreasing pause half-life, also shows the global difference between control and SSRP1-depleted cells (Figure 4C); at each time after triptolide addition, the number of genes showing paused Pol II was substantially decreased in cells depleted of SSRP1.

If FACT-dependent changes in PI measured by PRO-seq are due at least in part to a decrease in Pol II pause half-life, we would predict that highly paused genes, which showed the greatest decrease in PI, would also show the greatest decrease in pause half-life. To address this possibility, we compared changes in pause half-life following SSRP1 knockdown in highly, moderately, and lowly paused genes (Figure 4D). Although pause half-life was reduced in all three groups, highly paused genes indeed showed the greatest decrease in pause half-life. Taken together, these findings argue that FACT helps to maintain stable Pol II pausing across the genome.

DISCUSSION

In this report, we investigated roles of FACT during elongation by Pol II in *Drosophila* S2 cells. In addition to uncovering prominent roles for FACT in coordinating transcription-coupled chromatin alterations, we identified a role for FACT in promoter-proximal pausing, a key step in transcription activation in higher eukaryotes (Jonkers and Lis, 2015). FACT depletion results in the loss of transcriptionally engaged Pol II from pause sites at most genes, correlating with a marked decrease in the duration of Pol II pausing.

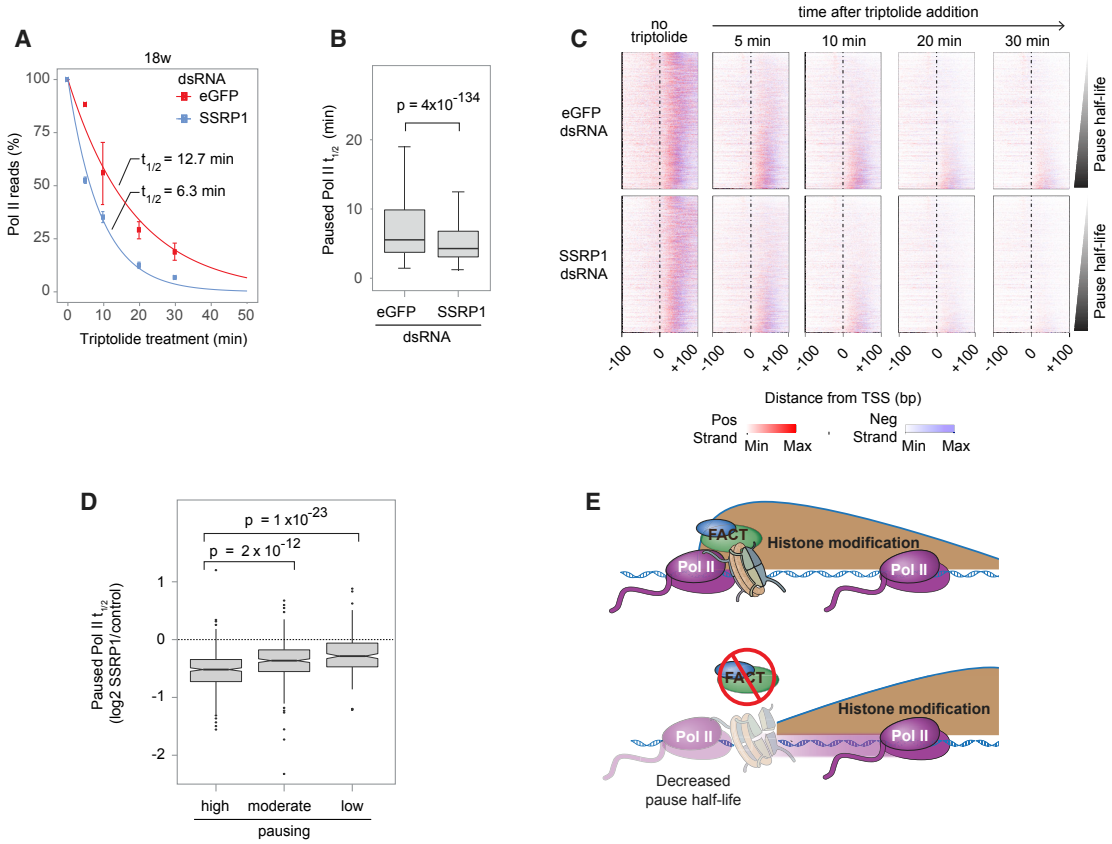

Figure 4. Paused Pol II Half-Life ($t_{1/2}$) Decreases in FACT-Depleted S2 Cells

(A–D) Chromatin from cells that had been treated with control dsRNA targeting EGFP or dsRNA targeting SSRP1 were incubated with 500-μM triptolide for 5, 10, 15, or 30 min or with 2% DMSO as control and subjected to ChIP-nexus using anti-Rpb3 antibodies. For each promoter where a typical Pol II ChIP-nexus footprint was observed (distance between positive and negative strand peak < 50 bp, position of Pol II footprint < 150 bp downstream of the TSS), spike-in normalized Pol II signal in a 51-bp window centered on the midpoint between paused Pol II positive and negative summits was determined, and the half-life of paused Pol II was calculated based on an exponential decay model.

(A) Pol II in the pausing window at 18w as a function of time after addition of triptolide, in cells treated with EGFP (red) or SSRP1 (blue) dsRNAs.

(B) Boxplot showing decreased paused Pol II half-life following SSRP1 depletion. p value was calculated with a two-sample Wilcoxon test, n = 998.

(C) Heatmaps of Pol II ChIP-nexus data at various times after triptolide addition in EGFP and SSRP1 dsRNA-treated cells.

(D) Boxplot showing fold change in pause half-life across highly paused (n = 411), moderately paused (n = 358), and lowly paused (n = 229) genes. p values were calculated using Wilcoxon rank sum test of pairwise comparisons.

(E) A model for FACT function in promoter-proximal pausing and transcription-coupled histone modifications. In control cells (top panel), the +1 nucleosome is stabilized by FACT (Ramachandran et al., 2017). The +1 nucleosome in turn helps to maintain Pol II in the vicinity of the promoter-proximal pause, and transcription-coupled histone modifications H3K4me3 and H3K36me3 are normally deposited. Upon depletion of FACT, the +1 nucleosome is destabilized, and Pol II spends less time at the promoter-proximal pause. Hence, methyltransferases associated with elongating Pol II are allowed less time to place marks, leading to a broadening of H3K4me3 and relative depletion of H3K36me3 from more 5′ portions of genes.

Together, these findings argue that FACT plays an important role in maintaining Pol II at promoter-proximal pause sites.

Paused Pol II can undergo multiple fates: it can enter productive elongation to complete synthesis of mature transcripts or it can terminate and leave the gene (Chiu et al., 2018; Erickson et al., 2018; Jonkers and Lis, 2015). At some genes, loss of PRO-seq reads at pause sites correlates with an increase in reads in the gene body, consistent with the possibility that at least some Pol II is prematurely released from its pause into productive elongation. At other genes, loss of PRO-seq reads at pause sites is not accompanied by an increase in gene body reads, raising the possibility that some paused Pol II at these genes terminates and fails to synthesize mature mRNA.

How FACT decreases Pol II pausing is presently not known; however, it is not difficult to imagine that its histone chaperone activity could play a role. Although FACT depletion in *Drosophila* S2 cells does not lead to the same substantial loss of nucleosomes at transcribed genes as in yeast, it is noteworthy that SSRP1 or Spt16 knockdown in S2 cells leads to transcription-dependent alterations in the +1 nucleosome consistent with partial unwrapping of the nucleosome or loss of one H2A-H2B dimer (Ramachandran et al., 2017). Thus, it is tempting to speculate that FACT helps to maintain an intact promoter-proximal nucleosome that acts as a barrier to slow pause release (Figure 4E). Alternatively, FACT's effect on pausing could be independent of histone chaperone activity. Indeed, FACT was reported to

influence transcription of naked DNA templates *in vitro* through functional interactions with factors that regulate pausing (Wada et al., 2000). In this case, however, FACT was found to cooperate with P-TEFb to overcome the activities of the pause-inducing factors DRB sensitivity-inducing factor (DSIF) and negative elongation factor (NELF), predicting that FACT depletion would increase, rather than decrease, pause duration.

FACT-dependent changes in elongation-coupled histone marks and promoter-proximal pausing could reflect independent activities of FACT or they could be causally related. Although future experiments will be required to distinguish between these possibilities, we favor the latter. Evidence suggests that changes in elongation rate, and hence the length of time Pol II spends in a particular region of the transcription unit, can affect the distribution of transcription-coupled modifications. H3K36me3 was shifted toward gene 5′ ends in human cells expressing a slowly elongating Pol II mutant (Fong et al., 2017). In addition, a comparison of elongation rate and H3K36me3 in mouse ES cells found that at genes where Pol II elongates more rapidly, H3K36me3 exhibits a relative depletion toward gene 5′ ends and a 5′ to 3′ shift in distribution much like that observed after FACT knockdown (Jonkers et al., 2014). Patterns of H3K4 methylation are also sensitive to elongation rate, being shifted in a 5′ direction in yeast expressing slowly elongating Pol II mutants, and in a 3′ direction in yeast expressing fast Pol II mutants (Soares et al., 2017). Further, in human cells, genes with broad peaks of H3K4me3, in which H3K4me3 is reduced at promoters and increased across transcribed regions, exhibit less promoter-proximal pausing. Blocking release from pausing with flavopiridol, an inhibitor of the P-TEFb kinase, resulted in narrower H3K4me3 peaks, suggesting that broadening of the H3K4me3 mark results from more rapid release of Pol II from the pause region (Chen et al., 2015). Notably, the broader H3K4me3 peaks seen in this study resemble those we observe after FACT knockdown. In light of these observations, the altered distribution of H3K36me3 and broadening of the H3K4me3 marks seen in FACT-depleted cells could be at least in part a consequence of decreased promoter-proximal pausing (Figure 4E).

STAR★METHODS

Detailed methods are provided in the online version of this paper and include the following:

- KEY RESOURCES TABLE
- LEAD CONTACT AND MATERIALS AVAILABILITY
- EXPERIMENTAL MODEL AND SUBJECT DETAILS
- METHOD DETAILS
  - Double-Stranded RNA (dsRNA) Mediated Knockdown of FACT
  - Antibodies
  - ChIP-Seq
  - ChIP-qPCR
  - PRO-Seq
  - RNA-Seq
  - Metaplots and Boxplots
  - ChIP-Seq and PRO-Seq Normalization
  - ChIP-Nexus and Measurement of Paused Pol II Half-Life
- QUANTIFICATION AND STATISTICAL ANALYSIS
  - Quantification of Western Blots
  - Quantification of H3 ChIP-qPCR Assays
  - Statistical Analysis
- DATA AND CODE AVAILABILITY

SUPPLEMENTAL INFORMATION

Supplemental Information can be found online at https://doi.org/10.1016/j.celrep.2019.05.099.

ACKNOWLEDGMENTS

We thank members of the Stowers Institute Molecular Biology and Tissue Culture Cores for library preparation and next-generation sequencing and for assistance with cell culture, respectively, and Mark Miller for help with the model figure and graphical abstract. This work was supported by funds from the Stowers Institute for Medical Research, United States, and by a grant to the Stowers Institute from the Helen Nelson Medical Research Fund at the Greater Kansas City Community Foundation, United States.

AUTHOR CONTRIBUTIONS

T.T.T., M.B., R.C.C., and J.W.C., developed the experimental design; T.T.T. performed most of the experiments; W.S. performed ChIP-nexus and analyzed the data; H.L. and X.G. were the lead analysts; Z.H.G. analyzed RNA-seq; M.B., B.A.S., A.D.C., and C.W.S. performed initial bioinformatic analyses; and R.L.G. provided essential reagents. T.T.T., R.C.C., and J.W.C. wrote the paper, and W.S. and J.Z. edited the paper. R.C.C., J.W.C., M.B., and J.Z. supervised the work. This work was done to fulfill, in part, a requirement for T.T.T.'s PhD thesis research as a student registered with the Open University.

DECLARATION OF INTERESTS

The authors declare no competing interests.

Received: April 24, 2018
Revised: April 22, 2019
Accepted: May 24, 2019
Published: June 25, 2019

REFERENCES

Belotserkovskaya, R., Oh, S., Bondarenko, V.A., Orphanides, G., Studitsky, V.M., and Reinberg, D. (2003). FACT facilitates transcription-dependent nucleosome alteration. Science *301*, 1090–1093.

Biswas, D., Yu, Y., Prall, M., Formosa, T., and Stillman, D.J. (2005). The yeast FACT complex has a role in transcriptional initiation. Mol. Cell. Biol. *25*, 5812–5822.

Brannan, K., and Bentley, D.L. (2012). Control of Transcriptional Elongation by RNA Polymerase II: A Retrospective. Genet. Res. Int. *2012*, 170173.

Brannan, K., Kim, H., Erickson, B., Glover-Cutter, K., Kim, S., Fong, N., Kiemele, L., Hansen, K., Davis, R., Lykke-Andersen, J., and Bentley, D.L. (2012). mRNA decapping factors and the exonuclease Xrn2 function in widespread premature termination of RNA polymerase II transcription. Mol. Cell *46*, 311–324.

Bruce, K., Myers, F.A., Mantouvalou, E., Lefevre, P., Greaves, I., Bonifer, C., Tremethick, D.J., Thorne, A.W., and Crane-Robinson, C. (2005). The replacement histone H2A.Z in a hyperacetylated form is a feature of active genes in the chicken. Nucleic Acids Res. *33*, 5633–5639.

Carter, D.R., Murray, J., Cheung, B.B., Gamble, L., Koach, J., Tsang, J., Sutton, S., Kalla, H., Syed, S., Gifford, A.J., et al. (2015). Therapeutic targeting of the MYC signal by inhibition of histone chaperone FACT in neuroblastoma. Sci. Transl. Med. *7*, 312ra176.

Chen, K., Chen, Z., Wu, D., Zhang, L., Lin, X., Su, J., Rodriguez, B., Xi, Y., Xia, Z., Chen, X., et al. (2015). Broad H3K4me3 is associated with increased transcription elongation and enhancer activity at tumor-suppressor genes. Nat. Genet. *47*, 1149–1157.

Chiu, A.C., Suzuki, H.I., Wu, X., Mahat, D.B., Kriz, A.J., and Sharp, P.A. (2018). Transcriptional Pause Sites Delineate Stable Nucleosome-Associated Premature Polyadenylation Suppressed by U1 snRNP. Mol. Cell *69*, 648–663.e7.

Chu, Y., Sutton, A., Sternglanz, R., and Prelich, G. (2006). The BUR1 cyclin-dependent protein kinase is required for the normal pattern of histone methylation by SET2. Mol. Cell. Biol. *26*, 3029–3038.

Core, L.J., Waterfall, J.J., and Lis, J.T. (2008). Nascent RNA sequencing reveals widespread pausing and divergent initiation at human promoters. Science *322*, 1845–1848.

Dermawan, J.K., Hitomi, M., Silver, D.J., Wu, Q., Sandlesh, P., Sloan, A.E., Purmal, A.A., Gurova, K.V., Rich, J.N., Lathia, J.D., et al. (2016). Pharmacological Targeting of the Histone Chaperone Complex FACT Preferentially Eliminates Glioblastoma Stem Cells and Prolongs Survival in Preclinical Models. Cancer Res. *76*, 2432–2442.

Ding, Q., He, K., Luo, T., Deng, Y., Wang, H., Liu, H., Zhang, J., Chen, K., Xiao, J., Duan, X., et al. (2016). SSRP1 Contributes to the Malignancy of Hepatocellular Carcinoma and Is Negatively Regulated by miR-497. Mol. Ther. *24*, 903–914.

Dobin, A., Davis, C.A., Schlesinger, F., Drenkow, J., Zaleski, C., Jha, S., Batut, P., Chaisson, M., and Gingeras, T.R. (2013). STAR: ultrafast universal RNA-seq aligner. Bioinformatics *29*, 15–21.

Erickson, B., Sheridan, R.M., Cortazar, M., and Bentley, D.L. (2018). Dynamic turnover of paused Pol II complexes at human promoters. Genes Dev. *32*, 1215–1225.

Feng, J., Gan, H., Eaton, M.L., Zhou, H., Li, S., Belsky, J.A., MacAlpine, D.M., Zhang, Z., and Li, Q. (2016). Noncoding Transcription Is a Driving Force for Nucleosome Instability in spt16 Mutant Cells. Mol. Cell. Biol. *36*, 1856–1867.

Fong, N., Saldi, T., Sheridan, R.M., Cortazar, M.A., and Bentley, D.L. (2017). RNA Pol II Dynamics Modulate Co-transcriptional Chromatin Modification, CTD Phosphorylation, and Transcriptional Direction. Mol. Cell *66*, 546–557.e3.

Formosa, T. (2008). FACT and the reorganized nucleosome. Mol. Biosyst. *4*, 1085–1093.

Garcia, H., Fleyshman, D., Kolesnikova, K., Safina, A., Commane, M., Paszkiewicz, G., Omelian, A., Morrison, C., and Gurova, K. (2011). Expression of FACT in mammalian tissues suggests its role in maintaining of undifferentiated state of cells. Oncotarget *2*, 783–796.

Garcia, H., Miecznikowski, J.C., Safina, A., Commane, M., Ruusulehto, A., Kilpinen, S., Leach, R.W., Attwood, K., Li, Y., Degan, S., et al. (2013). Facilitates chromatin transcription complex is an "accelerator" of tumor transformation and potential marker and target of aggressive cancers. Cell Rep. *4*, 159–173.

Gasparian, A.V., Burkhart, C.A., Purmal, A.A., Brodsky, L., Pal, M., Saranadasa, M., Bosykh, D.A., Commane, M., Guryanova, O.A., Pal, S., et al. (2011). Curaxins: anticancer compounds that simultaneously suppress NF-κB and activate p53 by targeting FACT. Sci. Transl. Med. *3*, 95ra74.

Guillemette, B., Bataille, A.R., Gévry, N., Adam, M., Blanchette, M., Robert, F., and Gaudreau, L. (2005). Variant histone H2A.Z is globally localized to the promoters of inactive yeast genes and regulates nucleosome positioning. PLoS Biol. *3*, e384.

Hossan, T., Nagarajan, S., Baumgart, S.J., Xie, W., Magallanes, R.T., Hernandez, C., Chiaroni, P.M., Indenbirken, D., Spitzner, M., Thomas-Chollier, M., et al. (2016). Histone Chaperone SSRP1 is Essential for Wnt Signaling Pathway Activity During Osteoblast Differentiation. Stem Cells *34*, 1369–1376.

Jamai, A., Puglisi, A., and Strubin, M. (2009). Histone chaperone spt16 promotes redeposition of the original h3-h4 histones evicted by elongating RNA polymerase. Mol. Cell *35*, 377–383.

Jeronimo, C., Watanabe, S., Kaplan, C.D., Peterson, C.L., and Robert, F. (2015). The Histone Chaperones FACT and Spt6 Restrict H2A.Z from Intragenic Locations. Mol. Cell *58*, 1113–1123.

Jonkers, I., and Lis, J.T. (2015). Getting up to speed with transcription elongation by RNA polymerase II. Nat. Rev. Mol. Cell Biol. *16*, 167–177.

Jonkers, I., Kwak, H., and Lis, J.T. (2014). Genome-wide dynamics of Pol II elongation and its interplay with promoter proximal pausing, chromatin, and exons. eLife *3*, e02407.

Kaplan, C.D., Laprade, L., and Winston, F. (2003). Transcription elongation factors repress transcription initiation from cryptic sites. Science *301*, 1096–1099.

Kharchenko, P.V., Alekseyenko, A.A., Schwartz, Y.B., Minoda, A., Riddle, N.C., Ernst, J., Sabo, P.J., Larschan, E., Gorchakov, A.A., Gu, T., et al. (2011). Comprehensive analysis of the chromatin landscape in Drosophila melanogaster. Nature *471*, 480–485.

Kwak, H., and Lis, J.T. (2013). Control of transcriptional elongation. Annu. Rev. Genet. *47*, 483–508.

Kwak, H., Fuda, N.J., Core, L.J., and Lis, J.T. (2013). Precise maps of RNA polymerase reveal how promoters direct initiation and pausing. Science *339*, 950–953.

Langmead, B., and Salzberg, S.L. (2012). Fast gapped-read alignment with Bowtie 2. Nat. Methods *9*, 357–359.

Leach, T.J., Mazzeo, M., Chotkowski, H.L., Madigan, J.P., Wotring, M.G., and Glaser, R.L. (2000). Histone H2A.Z is widely but nonrandomly distributed in chromosomes of Drosophila melanogaster. J. Biol. Chem. *275*, 23267–23272.

Lee, T.I., Johnstone, S.E., and Young, R.A. (2006). Chromatin immunoprecipitation and microarray-based analysis of protein location. Nat. Protoc. *1*, 729–748.

Li, H., Handsaker, B., Wysoker, A., Fennell, T., Ruan, J., Homer, N., Marth, G., Abecasis, G., and Durbin, R.; 1000 Genome Project Data Processing Subgroup (2009). The Sequence Alignment/Map format and SAMtools. Bioinformatics *25*, 2078–2079.

Liu, X., Kraus, W.L., and Bai, X. (2015). Ready, pause, go: regulation of RNA polymerase II pausing and release by cellular signaling pathways. Trends Biochem. Sci. *40*, 516–525.

Mahat, D.B., Kwak, H., Booth, G.T., Jonkers, I.H., Danko, C.G., Patel, R.K., Waters, C.T., Munson, K., Core, L.J., and Lis, J.T. (2016). Base-pair-resolution genome-wide mapping of active RNA polymerases using precision nuclear run-on (PRO-seq). Nat. Protoc. *11*, 1455–1476.

Mason, P.B., and Struhl, K. (2003). The FACT complex travels with elongating RNA polymerase II and is important for the fidelity of transcriptional initiation in vivo. Mol. Cell. Biol. *23*, 8323–8333.

Muse, G.W., Gilchrist, D.A., Nechaev, S., Shah, R., Parker, J.S., Grissom, S.F., Zeitlinger, J., and Adelman, K. (2007). RNA polymerase is poised for activation across the genome. Nat. Genet. *39*, 1507–1511.

Orphanides, G., LeRoy, G., Chang, C.H., Luse, D.S., and Reinberg, D. (1998). FACT, a factor that facilitates transcript elongation through nucleosomes. Cell *92*, 105–116.

Orphanides, G., Wu, W.H., Lane, W.S., Hampsey, M., and Reinberg, D. (1999). The chromatin-specific transcription elongation factor FACT comprises human SPT16 and SSRP1 proteins. Nature *400*, 284–288.

Raisner, R.M., Hartley, P.D., Meneghini, M.D., Bao, M.Z., Liu, C.L., Schreiber, S.L., Rando, O.J., and Madhani, H.D. (2005). Histone variant H2A.Z marks the 5′ ends of both active and inactive genes in euchromatin. Cell *123*, 233–248.

Ramachandran, S., Ahmad, K., and Henikoff, S. (2017). Transcription and Remodeling Produce Asymmetrically Unwrapped Nucleosomal Intermediates. Mol. Cell *68*, 1038–1053.e4.

Risso, D., Ngai, J., Speed, T.P., and Dudoit, S. (2014). Normalization of RNA-seq data using factor analysis of control genes or samples. Nat. Biotechnol. *32*, 896–902.

Robinson, J.T., Thorvaldsdóttir, H., Winckler, W., Guttman, M., Lander, E.S., Getz, G., and Mesirov, J.P. (2011). Integrative genomics viewer. Nat. Biotechnol. *29*, 24–26.

Robinson, M.D., McCarthy, D.J., and Smyth, G.K. (2010). edgeR: a Bioconductor package for differential expression analysis of digital gene expression data. Bioinformatics *26*, 139–140.

Safina, A., Garcia, H., Commane, M., Guryanova, O., Degan, S., Kolesnikova, K., and Gurova, K.V. (2013). Complex mutual regulation of facilitates chromatin transcription (FACT) subunits on both mRNA and protein levels in human cells. Cell Cycle *12*, 2423–2434.

Saunders, A., Werner, J., Andrulis, E.D., Nakayama, T., Hirose, S., Reinberg, D., and Lis, J.T. (2003). Tracking FACT and the RNA polymerase II elongation complex through chromatin in vivo. Science *301*, 1094–1096.

Schwabish, M.A., and Struhl, K. (2004). Evidence for eviction and rapid deposition of histones upon transcriptional elongation by RNA polymerase II. Mol. Cell. Biol. *24*, 10111–10117.

Shao, W., and Zeitlinger, J. (2017). Paused RNA polymerase II inhibits new transcriptional initiation. Nat. Genet. *49*, 1045–1051.

Shilatifard, A. (2012). The COMPASS family of histone H3K4 methylases: mechanisms of regulation in development and disease pathogenesis. Annu. Rev. Biochem. *81*, 65–95.

Soares, L.M., He, P.C., Chun, Y., Suh, H., Kim, T., and Buratowski, S. (2017). Determinants of Histone H3K4 Methylation Patterns. Mol. Cell *68*, 773–785.e6.

Stanlie, A., Aida, M., Muramatsu, M., Honjo, T., and Begum, N.A. (2010). Histone3 lysine4 trimethylation regulated by the facilitates chromatin transcription complex is critical for DNA cleavage in class switch recombination. Proc. Natl. Acad. Sci. USA *107*, 22190–22195.

Titov, D.V., Gilman, B., He, Q.L., Bhat, S., Low, W.K., Dang, Y., Smeaton, M., Demain, A.L., Miller, P.S., Kugel, J.F., et al. (2011). XPB, a subunit of TFIIH, is a target of the natural product triptolide. Nat. Chem. Biol. *7*, 182–188.

Venkatesh, S., and Workman, J.L. (2013). Set2 mediated H3 lysine 36 methylation: regulation of transcription elongation and implications in organismal development. Wiley Interdiscip. Rev. Dev. Biol. *2*, 685–700.

Vispé, S., DeVries, L., Créancier, L., Besse, J., Bréand, S., Hobson, D.J., Svejstrup, J.Q., Annereau, J.P., Cussac, D., Dumontet, C., et al. (2009). Triptolide is an inhibitor of RNA polymerase I and II-dependent transcription leading predominantly to down-regulation of short-lived mRNA. Mol. Cancer Ther. *8*, 2780–2790.

Voth, W.P., Takahata, S., Nishikawa, J.L., Metcalfe, B.M., Näär, A.M., and Stillman, D.J. (2014). A role for FACT in repopulation of nucleosomes at inducible genes. PLoS ONE *9*, e84092.

Wada, T., Orphanides, G., Hasegawa, J., Kim, D.K., Shima, D., Yamaguchi, Y., Fukuda, A., Hisatake, K., Oh, S., Reinberg, D., and Handa, H. (2000). FACT relieves DSIF/NELF-mediated inhibition of transcriptional elongation and reveals functional differences between P-TEFb and TFIIH. Mol. Cell *5*, 1067–1072.

Wagschal, A., Rousset, E., Basavarajaiah, P., Contreras, X., Harwig, A., Laurent-Chabalier, S., Nakamura, M., Chen, X., Zhang, K., Meziane, O., et al. (2012). Microprocessor, Setx, Xrn2, and Rrp6 co-operate to induce premature termination of transcription by RNAPII. Cell *150*, 1147–1157.

Wickham, H. (2009). ggplot2: Elegant Graphics for Data Analysis (Springer).

Woo, H., Dam Ha, S., Lee, S.B., Buratowski, S., and Kim, T. (2017). Modulation of gene expression dynamics by co-transcriptional histone methylations. Exp. Mol. Med. *49*, e326.

Xin, H., Takahata, S., Blanksma, M., McCullough, L., Stillman, D.J., and Formosa, T. (2009). yFACT induces global accessibility of nucleosomal DNA without H2A-H2B displacement. Mol. Cell *35*, 365–376.

Zeitlinger, J., Stark, A., Kellis, M., Hong, J.W., Nechaev, S., Adelman, K., Levine, M., and Young, R.A. (2007). RNA polymerase stalling at developmental control genes in the Drosophila melanogaster embryo. Nat. Genet. *39*, 1512–1516.

Zhang, H., Roberts, D.N., and Cairns, B.R. (2005). Genome-wide dynamics of Htz1, a histone H2A variant that poises repressed/basal promoters for activation through histone loss. Cell *123*, 219–231.

Zhang, Y., Liu, T., Meyer, C.A., Eeckhoute, J., Johnson, D.S., Bernstein, B.E., Nusbaum, C., Myers, R.M., Brown, M., Li, W., and Liu, X.S. (2008). Model-based analysis of ChIP-Seq (MACS). Genome Biol. *9*, R137.

STAR★METHODS

KEY RESOURCES TABLE

REAGENT or RESOURCE	SOURCE	IDENTIFIER
Antibodies		
Rabbit polyclonal anti-Spt16	This paper	N/A
Rabbit polyclonal anti-SSRP1	This paper	N/A
Rabbit polyclonal anti-H2Av serum	Leach et al., 2000	N/A
Rabbit polyclonal anti-H3	Abcam	Cat# ab1791; RRID:AB_302613
Rabbit polyclonal anti-H3K4me3	Abcam	Cat# ab8580; RRID:AB_306649
Rabbit polyclonal anti-H3K36me3	Abcam	Cat# ab9050; RRID:AB_306966
Rabbit polyclonal anti-Rpb3 (*Drosophila*)	Julia Zeitlinger Lab (Shao and Zeitlinger, 2017)	Zeitlinger Lab #163185-50
Rabbit polyclonal anti-Rpb1 N-20	Santa Cruz	Cat# sc-899X; RRID:AB_632359
Rabbit IgG	Santa Cruz	Cat# sc-2027; RRID:AB_737197
Mouse monoclonal anti-α-tubulin DM1A	Sigma	Cat# T9026; RRID:AB_477593
Alexa Fluor® 680 goat anti-rabbit IgG (H+L)	Life Technologies (Invitrogen)	Cat# A-21076; RRID:AB_141386
IRdye® 800CW Donkey anti-Mouse IgG(H+L)	LI-COR	Cat# 926-32212; RRID:AB_621847
Chemicals, Peptides, and Recombinant Proteins		
Proteinase K Solution (20 mg/ml)	Invitrogen	Cat# 25530-049
Protease Inhibitor Cocktail	Sigma	Cat# P8849
RNaseA	Sigma	Cat# R6513
Protein A/G Magnetic Beads	Invitrogen	Cat# 88803
Phenol:Chloroform:Isoamyl Alcohol 25:24:1	Sigma	Cat# P3803
Protein G Magnetic Beads	Life Technologies	Cat# REF 10004D
Amplitaq	Roche Applied Science	Cat# 11435094001
Triptolide	TOCRIS Bioscience	Cat# 3253
Quick T4 DNA ligase	New England BioLabs	Cat# M2200
Klenow fragment	New England BioLabs	Cat# M0212
T4 DNA polymerase	New England BioLabs	Cat# M0203
lambda exonuclease	New England BioLabs	Cat# M0262
RecJf exonuclease	New England BioLabs	Cat# M0264
CircLigase	Epicenter	Cat# CL4115K
SUPERaseIN	Ambion	Cat# AM2696
Biotin-11-ATP	PerkinElmer	Cat# NEL544001EA
Biotin-11-GTP	PerkinElmer	Cat# NEL545001EA
Biotin-11-CTP	PerkinElmer	Cat# NEL542001EA
Biotin-11-UTP	PerkinElmer	Cat# NEL543001EA
Trizol LS	Invitrogen	Cat# 10296-028
CNBr-Sepharose 4B	GE Healthcare	Cat# 17-0430-1
RNase inhibitor	Ambion	Cat# AM2696
Streptavidin M280 beads	Life Technologies	Cat# 11206D
Dynabeads Protein G	ThermoFisher Scientific	Cat# 10003D
Dynabeads Protein A	ThermoFisher Scientific	Cat# 10001D
Critical Commercial Assays		
QiaQuick PCR purification kit	QIAGEN	Cat# 28104
RNeasy mini kit	QIAGEN	Cat# 74106
KAPA HTP library preparation kit	Kapa Biosystems	Cat# KK8234
SPRIselect double side size selection kit	Beckman Coulter	Cat# B23319

(*Continued on next page*)

Continued

REAGENT or RESOURCE	SOURCE	IDENTIFIER
2% Agarose Gel Cassette, Dye-Free (Cassette type: 2% DF Marker L)	Sage Science	Cat# CDF2010
NEBNext End Repair Module	New England BioLabs	Cat# E6050
NEBNext dA-Tailing Module	New England BioLabs	Cat# E6053
TruSeq Standard mRNA LT Sample Prep Kit, 48; Set A	Illumina	Cat# RS-122-2101
NEBNext High-Fidelity 2X PCR Master Mix	New England BioLabs	Cat# M0541
Deposited Data		
Raw and analyzed sequencing data	This paper	GEO: GSE129236
Raw data from Figures 1A and S2	This paper	https://www.stowers.org/research/publications/LIBPB-1282
Experimental Models: Cell Lines		
Drosophila melanogaster Schneider 2 cells	*Drosophila* Genomics Resource Center (DGRC)	Cat# 6, RRID:CVCL_Z232
GM12878 EBV-immortalized lymphoblastoid cells	Coriell	Cat# GM12878
Oligonucleotides		
3′ RNA adaptor (RNase-free, HPLC purified): 5′Phos/rGrArU rCrGrU rCrGrG rArCrU rGrUrA rGrArA rCrUrC rUrGrA rArC/3′Inverted dT	Integrated DNA Technologies	N/A
5′ RNA adaptor (RNase-free, HPLC purified): rCrCrU rUrGrG rCrArC rCrCrG rArGrA rArUrU rCrCrA	Integrated DNA Technologies	N/A
Illumina RP1 primer (RNase-free, HPLC purified): AAT GAT ACG GCG ACC ACC GAG ATC TAC ACG TTC AGA GTT CTA CAG TCC GA	Integrated DNA Technologies	N/A
Illumina RPI4 index primer (RNase-free, HPLC purified): CAA GCA GAA GAC GGC ATA CGA GAT TGG TCA GTG ACT GGA GTT CCT TGG CAC CCG AGA ATT CCA	Integrated DNA Technologies	N/A
Illumina RPI5 index primer (RNase-free, HPLC purified): CAA GCA GAA GAC GGC ATA CGA GAT CAC TGT GTG ACT GGA GTT CCT TGG CAC CCG AGA ATT CCA	Integrated DNA Technologies	N/A
Illumina RPI6 index primer (RNase-free, HPLC purified): CAA GCA GAA GAC GGC ATA CGA GAT ATT GGC GTG ACT GGA GTT CCT TGG CAC CCG AGA ATT CCA	Integrated DNA Technologies	N/A
Illumina RPI7 index primer (RNase-free, HPLC purified): CAA GCA GAA GAC GGC ATA CGA GAT GAT CTG GTG ACT GGA GTT CCT TGG CAC CCG AGA ATT CCA	Integrated DNA Technologies	N/A
Oligonucleotides for ChIP-nexus, see Table S1	This paper	N/A
Primers for ChIP-qPCR, see Table S2	This paper	N/A
Primers for dsRNA-mediated knockdown T7 templates, see Table S3	This paper	N/A
Recombinant DNA		
pDONR221-SSRP1	This paper	N/A
pDONR221-Spt16	This paper	N/A
pDONR221	ThermoFisher Scientific	Cat# 12536017
Software and Algorithms		
Illumina bcl2fastq2 v2.18	Illumina	https://www.illumina.com/
SAMtools	Li et al., 2009	http://samtools.sourceforge.net/
Bowtie2 version 2.2.9	Langmead and Salzberg, 2012	http://bowtie-bio.sourceforge.net/bowtie2/index.shtml

(*Continued on next page*)

Continued

REAGENT or RESOURCE	SOURCE	IDENTIFIER
ggplot2	Wickham, 2009	https://ggplot2.tidyverse.org/
MACS2 version 2.1.1.20160309	Zhang et al., 2008	https://github.com/taoliu/MACS/
IGV 2.3	Robinson et al., 2011	http://software.broadinstitute.org/software/igv/igv2.3
STAR version 2.5.2b	Dobin et al., 2013	https://github.com/alexdobin/STAR
edgeR	Robinson et al., 2010	http://bioconductor.org/packages/release/bioc/html/edgeR.html
RUVSeq	Risso et al., 2014	https://bioconductor.org/packages/release/bioc/html/RUVSeq.html
Image Studio Version 5.2.	LI-COR Biosciences	N/A
Other		
Odyssey Infrared Imaging System, Model 9120	LI-COR Biosciences	N/A
Misonix S-3000 Sonicator	QSonica, LLC	N/A
HiSeq 2500-DNA Sequencer	Illumina	N/A
Pippen Prep	Sage Science	N/A
Agilent 2100 Bioanalyzer	Agilent Technologies	Cat# G2939BA
Mastercycler EP Gradient-Thermal Cycler	Eppendorf North America	N/A
NanoDrop-2000C Spectrophotometer	Thermo Fisher Scientific	Cat# ND-2000C
Bioruptor® Pico Sonicator	Diagenode, Inc.	Cat# B01060010
Thermomixer 5350	Eppendorf North America	N/A

LEAD CONTACT AND MATERIALS AVAILABILITY

Further information and requests for resources and reagents should be directed to and will be fulfilled by the Lead Contact, Joan Conaway (jlc@stowers.org).

EXPERIMENTAL MODEL AND SUBJECT DETAILS

Drosophila S2 cells (RRID:CVCL_Z232) were grown at 25°C in Schneider's media (GIBCO #21720) supplemented with 10% heat-inactivated fetal bovine serum (PAA Laboratories #A15-701).

METHOD DETAILS

Double-Stranded RNA (dsRNA) Mediated Knockdown of FACT

Double-stranded RNA-mediated knockdowns were performed in *Drosophila* embryonic S2 cells using either one of the two non-overlapping double stranded RNAs targeting either SSRP1 or Spt16. Double stranded eGFP RNA was used as a non-targeting control to rule out off-target effects. DsRNAs were generated as follows: SSRP1 and Spt16 coding sequences were PCR-amplified from S2 cell-derived cDNA using attB modified custom primers *attB*1-SSRP1.fwd / *attB*2-SSRP1.rev and *attB*1-Spt16.fwd / *attB*2-Spt16.rev, respectively. PCR products were introduced into Gateway pDONR221 vectors to generate pDONR221-SSRP1 and pDONR221-Spt16. To generate templates for dsRNA synthesis, 500 μl PCR reaction mixtures containing 25 units of Amplitaq (Roche Applied Science), 1X Amplitaq buffer (Roche), 200 μM each dNTP, 0.75 μM each of the forward and reverse primers, and pDONR221-SSRP1 or pDONR221-Spt16 were aliquoted into eight 0.25ml PCR tubes and amplified using an Eppendorf thermocycler using the following conditions: initial denaturation at 94°C for3 min, followed by 35 cycles of 94°C for 30 s, 55°C for 30 s and 72°C for 1 min and a 10 min final extension at 72°C. Following PCR amplification, the eight reactions were pooled, and the amplicons were purified using the QiaQuick PCR purification kit (QIAGEN). Amplicons were eluted from the column into 50 μl of TE (10 mM Tris HCl pH 7.5, 1 mM EDTA). DNA concentration of the final products were measured using a NanoDrop2000c Spectrophotometer, and the quality of the amplicons assessed by electrophoresis on a 2% agarose gel in 0.5 X TBE.

All experiments were performed in duplicate. For RNA-seq, ChIP-seq, and ChIP-nexus experiments, about 2×10^6 cells were seeded in each well of a 6-well dish (35 mm) for each replica. Cells were incubated at 25°C for 30 min to allow cells to attach to the bottom of the plate, and 10 μg dsRNA was added to each well. For PRO-seq, about 12×10^6 cells were seeded in a 100 mm dish for each replica and incubated at 25°C for 30 min. Cells were then treated by adding 60 μg dsRNA to each dish. After 48 hours at 25°C, a second dose of 10 μg or 60 μg of dsRNA was added to cells for RNA-seq and ChIP-Seq or PRO-seq, respectively. 48 hours

later, the cells were harvested to study the loss of function phenotypes. For RNA-seq and ChIP-seq, cells were washed twice by re-suspension in 1 mL phosphate buffered saline (PBS) followed by centrifugation at 1500 x g for 5 min at 4°C and then resuspended in 500 μL PBS. For PRO-seq, cells were washed twice by resuspension in 10 mL PBS followed by centrifugation at 1000 x g for 5 min in a swinging bucket rotor. After the last wash, nuclei were prepared for PRO-seq as described below. For all experiments, SSRP1 and Spt16 knockdown efficiency was confirmed by western blotting with anti-SSRP1 or anti-Spt16 primary antibodies and Alexa Fluor® 680 goat anti-rabbit IgG (H+L) secondary antibodies. Tubulin (loading control) was detected using anti-tubulin mouse monoclonal primary and IRdye800 Donkey anti-Mouse IgG(H+L) secondary antibodies. Blots were visualized using a LI-COR Odyssey Imaging System.

Antibodies

Custom antibodies against full length, bacterially expressed Spt16 and SSRP1 that had been purified from inclusion bodies were raised in rabbits (YenZym Antibodies, LLC) and affinity purified from antisera using full length Spt16 and SSRP1 coupled to CNBr-Sepharose 4B (GE Healthcare) according to the manufacturer's instructions. Other antibodies included rabbit polyclonal antibodies against the full-length *Drosophila* Pol II subunit Rpb3 (Zeitlinger lab; Shao and Zeitlinger, 2017), H3 (ab1791, Abcam), H3K36me3 (ab9050, Abcam), H3K4me3 (ab8580, Abcam), and H2Av anti-serum (Leach et al., 2000).

ChIP-Seq

Chromatin immunoprecipitation was performed essentially as described (Lee et al., 2006). Formaldehyde crosslinking was performed by adding an equal volume of 2% formaldehyde solution (900 μL 16% formaldehyde in 7.3 mL 1 X PBS) to the resuspended cells and incubated at room temperature for 20 min. The formaldehyde crosslinking was quenched by adding 1/20 volume of 2.5 M glycine to the cells in suspension. The cells were then washed twice using ice-cold 0.125 M glycine in 1 X PBS. Next, the cell pellet was resuspended in 500 μL buffer A2 (15 mM HEPES pH 7.5, 140 mM NaCl, 1 mM EDTA, 0.5 mM EGTA, 1% Triton X-100, 0.1% Sodium deoxycholate, 1% SDS, 0.5% N-lauroylsarcosine, 1/200 volume protease inhibitor cocktail (Sigma). The nuclei were pelleted by spinning at 3500 x g for 5min at 4°C. Nuclei were resuspended in 800 μl Buffer A2 and sonicated using a Misonix 3000 sonicator at 4°C using output power 3 (9 w power) for 10 cycles (where each cycle is a 10 s burst of sonication, followed by a 60 s pause) and spun at 14000 rpm at 4°C for 10 min. A 30 μl aliquot of the sheared chromatin (supernatant) was saved as input sample to normalize the eluate signals and to check the sonication efficiency.

Prior to the immunoprecipitation, Protein A/G (Invitrogen) or Protein G (Life Technologies) magnetic beads were washed twice using BSA solution (0.5% BSA in 1X PBS). 10 μg anti- Rpb3, H3, and H2Av serum were coupled to Protein G beads, while anti-H3K36me3, H3K4me3, normal Rabbit IgG (Santa Cruz), SSRP1 (This paper), and Spt16 (This paper), were coupled to Protein A/G magnetic beads by incubating in BSA solution (0.5% BSA in 1X PBS) for 4 hours at 4°C on a rotator. The antibody-conjugated beads were then washed twice using 0.5% BSA in 1X PBS. The sheared chromatin was then added to the antibody-conjugated Protein A/G or Protein G beads and incubated overnight at 4°C. The beads-antibody-protein complexes were washed twice with 20 mM Tris-HCl, pH 8.0, 150 mM NaCl, 2 mM EDTA, 1% Triton X-100, once with 20 mM Tris-HCl, 500 mM NaCl, 2 mM EDTA, 1% Triton X-100, and once with 20 mM Tris-HCl, pH 8.0, 250 mM LiCl, 1 mM, 1% Triton X-100, 0.1% NP-40, 0.5% sodium deoxycholate at 4°C. Washed bead-antibody-protein complexes were resuspended in 150 μl elution buffer (50 mM Tris-HCl pH 8.0, 10 mM EDTA, 1% SDS), 150 μL TE (10 mM Tris-HCl, pH 8.0, 1 mM EDTA), and 4 μL of 10 μg/μl RNaseA (Sigma). In parallel, 120 μL elution buffer, 150 μL TE, and 4 μL of 10 μg/μl RNaseA were added to 30 μl of each input sample. Input samples and bead-antibody-protein complexes were then incubated in a Thermomixer at 37°C with shaking for 30 min. In order to digest the proteins and reverse the crosslinking, 2 μL of Proteinase K solution (Invitrogen) was added to the eluate and incubated overnight at 65°C while shaking on the thermomixer. DNA was purified using Phenol:Chloroform:Isoamyl Alcohol 25:24:1 (Sigma), precipitated using ethanol, and resuspended in nuclease free water. Libraries from the ChIPed DNA were prepared using the KAPA HTP kit (Kapa Biosystems), size selected using the SPRIselect double side size selection kit (Beckman Coulter) and sequenced on the Illumina HiSeq 2500 platform.

The ~30 million reads from each experiment were demultiplexed into Fastq format allowing up to one mismatch using Illumina bcl2fastq2 v2.18. Reads were aligned to UCSC genome dm6 with Bowtie2 version 2.2.9 (Langmead and Salzberg, 2012) with default settings. Reads were extended to 150 bases toward the interior of the sequenced fragment and normalized to total reads aligned (reads per million; RPM). FACT and Rpb3 peaks were called by MACS2, version 2.1.1.20160309 (Zhang et al., 2008), broad peak at $q < 0.1$. Peaks were annotated to the nearest gene; peaks within 200 bp upstream to 1000 bp downstream of TSSs were annotated as TSS and early transcribed regions.

ChIP-qPCR

To assess the effect of SSRP1 or Spt16 knockdown on H3 occupancy at promoter regions and within the gene bodies of selected genes, we performed anti-H3 ChIP as described above under ChIP-seq using chromatin from cells treated with eGFP, SSRP1, or Spt16 dsRNAs. IP and input samples were analyzed by quantitative real-time PCR (qPCR) using PerfeCTa SYBR Green FastMix Low ROX (Quanta bio) in a QantStudio 7 Flex-Thermal Cycler (Life Technologies-Applied Biosystems). Table S2 lists PCR primers used to amplify regions at the transcription start sites and within the gene bodies of Inos, Droj2, and 18w and within the gene body of Hsp22, as well as in two transcriptionally inactive genomic regions.

PRO-Seq

The PRO-seq procedure and library preparation were performed as previously described (Kwak and Lis, 2013; Mahat et al., 2016). Briefly, nuclei were isolated from the washed cells by resuspending gently in 5ml ice cold douncing buffer (10 mM Tris-HCl pH 7.4, 300 mM sucrose, 3 mM CaCl2, 2 mM MgCl2, 0.1% Triton X-100, 0.5 mM DTT, 1 tablet of protease inhibitors cocktail (Roche) per 50 ml, 4 u/ml RNase inhibitor (SUPERaseIN), incubated on ice for 5 min and dounced until 90% of cells were lysed (from 5-25) in a 5 mL capacity Dounce homogenizer. Nuclei were then pelleted at 1000 x g for 4 min in a swinging bucket at 4°C, washed twice using 10 mL douncing buffer and resuspended in storage buffer (10 mM Tris-HCl pH 8.0, 25% (vol/vol) glycerol, 5 mM magnesium acetate, 0.1 mM EDTA, 5 mM DTT) at a concentration of 20×10^6 nuclei/100 μl. The isolated nuclei from the two biological replicates for each condition were flash frozen in liquid nitrogen and stored at −80°C.

To perform the 4-biotin run-on assay, 20×10^6 nuclei in 100 μl storage buffer were mixed thoroughly with an equal volume of pre-heated (30°C) 2 X Nuclear Run-On master mix (10 mM Tris HCl pH 8.0, 5 mM $MgCl_2$, 300 mM KCl, 1 mM DTT, 0.8 u/μl RNase inhibitor (Ambion), 1% Sarkosyl and 50 μM each of Biotin-11-ATP, Biotin-11-GTP, Biotin-11-CTP, Biotin-11-UTP, all from PerkinElmer, and incubated for 3 min at 30°C in a heat block. The nascent RNA was extracted using Trizol LS (Invitrogen) and precipitated using 2.5 volumes of 100% ethanol. The purified RNA was fragmented by base hydrolysis in 0.2 N NaOH and enriched for biotinylated nascent transcripts by purifying in streptavidin-coated magnetic beads (Life Technologies). After the 3′ RNA adaptors were ligated to the fragmented RNAs, a second round of biotin-streptavidin purification was performed. The mRNA cap was then removed and the reverse 5′ RNA adaptor ligated. A third biotin affinity purification was performed, and the cloned products were reverse transcribed using RP1 primer. Primers RPI4, RPI5, RPI6 and RPI7 were used to barcode cDNAs from eGFPdsRNA_rep1 (Non-targeting control, replicate 1), eGFPdsRNA_rep2(Non-targeting control, replicate 2), SSRP1kda1 (SSRP1 dsRNA mediated knockdown, replicate 1), and SSRP1kda2 (SSRP1 dsRNA mediated knockdown, replicate 2) respectively.

PCR amplicons of 140 bp to 350 bp were selected using the 2% Agarose Gel Cassette, Dye-Free (Sage Science, CDF2010, Cassette type: 2% DF Marker L) on the Pippen Prep (Sage Science, Software: v.5.8) instrument. Equimolar concentrations of library fractions were then pooled together and sequenced using a mid-output flow cell on the Illlumina NextSeq 500 platform.

Raw reads were demultiplexed into Fastq format allowing up to one mismatch using Illumina bcl2fastq2 v2.18. The adaptor sequence 5′-TGGAATTCTCGGGTGCCAAGG-3′ was removed, and reads were trimmed to 36 bp. Reads with length less than 15 bp after trimming were removed. After reverse-complementing, reads were aligned to UCSC genome dm6 with Bowtie2 version 2.2.9 with default settings. Normalized coverage tracks were generated by applying a normalization factor calculated from reads aligned to the previously characterized transcriptionally silent regions (Kharchenko et al., 2011). Normalized bigwig files were then used for downstream analysis.

Pausing indices (the ratio of promoter coverage, defined as −50 to +150 around the TSS, versus the gene body, defined as +300 from the TSS to the end of the transcript) were calculated as described (Kwak et al., 2013). Genes were divided into three equal groups designated highly paused ($PI \geq 23.5$), moderately paused, ($3.3 < PI < 23.5$), and lowly paused ($PI \leq 3.3$). Genes that were less than 500 bp in length, overlapped other genes or were within 200 nt of nearby genes were excluded from the downstream analysis. For genes with more than one annotated TSS, the TSS with highest PRO-seq coverage was selected. We also excluded genes with less than 1 RPKM PRO-seq signal in the promoter region in order to exclude non-active genes.

RNA-Seq

At the end of the 4-day knockdown, *Drosophila* S2 cells were harvested. Human HEK293T cells were added to the harvested S2 cells (0.8x10e6 human cells / 15x10e6 S2 cells) as spike-in control. Each pool of S2 and HEK293T cells was washed twice using 1 X PBS. Total RNA was extracted using the QIAGEN RNeasy mini kit (QIAGEN) following the manufacturer's protocol. The quantity and integrity of the isolated RNA were assessed using the Agilent Bioanalyzer. PolyA+ RNA libraries were prepared following the Illumina TruSeq Stranded mRNA sample preparation protocol (Illumina) using the TruSeq Standard mRNA LT Sample Prep Kit, 48; Set A (Illumina). Libraries were sized-selected using dye-free 2% agarose gel cassettes with a Pippen Prep (Sage Science) and validated using Agilent 2100 Bioanalyzer. Barcoded libraries were pooled together and subjected to sequencing on a HiSeq 2500-DNA Sequencer to generate 50 bp single end reads.

Raw reads were demultiplexed into Fastq format allowing up to one mismatch using Illumina bcl2fastq2 v2.18. Reads were aligned using default settings to a combined dm6-hg38 genome with STAR version 2.5.2b (Dobin et al., 2013), using Ensembl 84 gene models. The RUVg method (Risso et al., 2014) was applied to remove unwanted variation in gene counts. Spike-in genes with at least 100 counts in all samples were used as negative control genes. RUVg yields factors of unwanted variation for each sample, which are incorporated as a term in the edgeR negative binomial GLM (Robinson et al., 2010) to perform differential gene expression analysis. Genes with reads of more than 1 count per million (CPM) in any two samples were included in downstream analyses.

Metaplots and Boxplots

Metaplots showing average gene profiles of SSRP1 and Spt16 occupancy include 876 genes that overlap SSRP1 or Spt16 high confidence peaks (MACS2 FDR $\leq 10^{-2}$; fold change ≥ 1.5); boxplots comparing FACT and Rpb3 occupancy show data from the same set of genes. H3, H2A.v, H3K4me3, and PRO-seq metaplots show normalized average gene profiles of transcripts (n = 1556) that are longer than 1500 bp and separated from other transcripts by at least 200 base pairs; only transcripts with PRO-seq coverage in control, eGFP dsRNA-treated cells of more than 1 RPKM in the region −50 to +150 relative to dm6 annotated TSSs were included. For

genes with more than one annotated TSS, the TSS with highest PRO-Seq coverage was selected. The indicated regions upstream and downstream of TSS and TES were plotted. The remainder of gene bodies were scaled to a length of 1000 bp, and data were averaged using 10 bp bins. Boxplots in Figures 2, 3, S3, and S4 include data from transcripts (n = 2023) that are longer than 1000 bp, separated from other transcripts by at least 200 bp, and have PRO-seq coverage in control cells of more than 1 RPKM in the −50 to +150 region. Plots were generated with R package ggplot2 (Wickham, 2009).

ChIP-Seq and PRO-Seq Normalization

To compare transcription-dependent changes in H3, H2A.v, H3K4me3, H3K36me3, and PRO-seq datasets from control and FACT-depleted cells, we normalized datasets to ChIP or PRO-seq signals at regions of transcriptionally silent, intergenic euchromatin regions, where FACT depletion is expected to have minimal effect on chromatin architecture. These transcriptionally silent, intergenic euchromatin regions were lifted from dm3 to dm6 genome annotation. The scaling factor for each dataset (Table S4) was based on the number of reads in 444 silent domains (state 9) (Kharchenko et al., 2011) that are longer than 1 kb and do not overlap with annotated genes.

ChIP-Nexus and Measurement of Paused Pol II Half-Life

The ChIP-nexus procedure and library preparation were performed for each of the two biological replicates of each knockdown and control conditions as previously described (Shao and Zeitlinger, 2017). Briefly, cells were treated with triptolide at room temperature for 5, 10, 15, and 30 min and 2% DMSO as control. Each sample was then fixed with 1% formaldehyde at room temperature for 10 min, washed with cold PBS, incubated with Orlando and Paro's Buffer A (0.25% Triton X-100, 10 mM EDTA, 0.5 mM EGTA, 10 mM Tris-HCl, pH 8.0) for 10 min at room temperature with rotation, and then centrifuged and re-suspended in S2-RIPA buffer (10 mM Tris-HCl, pH 8.0; 140 mM NaCl; 0.1% SDS; 0.1% sodium deoxycholate; 0.5% sarkosyl; 1% Triton X-100). Sonication was performed with a Bioruptor® Pico sonicator for five rounds of 30 s on and 30 s off.

For each ChIP-nexus experiment, chromatin extracts from 10^7 S2 cells were incubated with a 1:1 mixture of Dynabeads Protein A (ThermoFisher Scientific) and Dynabeads Protein G (ThermoFisher Scientific) coupled to custom-made antibodies against *Drosophila* Pol II Rpb3 subunit and washed with nexus washing buffer A to D (wash buffer A: 10 mM Tris-EDTA, 0.1% Triton X-100, wash buffer B: 150 mM NaCl, 20 mM Tris-HCl, pH 8.0, 5 mM EDTA, 5.2% sucrose, 1.0% Triton X-100, 0.2% SDS, wash buffer C: 250 mM NaCl, 5 mM Tris-HCl, pH 8.0, 25 mM HEPES, 0.5% Triton X-100, 0.05% sodium deoxycholate, 0.5 mM EDTA, wash buffer D: 250 mM LiCl, 0.5% IGEPAL CA-630, 10 mM Tris-HCl, pH 8.0, 0.5% sodium deoxycholate, 10 mM EDTA). To control for the loss of Pol II ChIP signal after triptolide treatment, a spike-in control was prepared by incubating human chromatin extracts from GM12878 cells with a 1:1 mixture of Dynabeads Protein A and Dynabeads Protein G coupled to antibodies against human Pol II (N20, Santa Cruz) followed by washing with nexus washing buffers A to D. A fixed amount of Dynabeads and human Pol II ChIP mixture was then spiked into each S2 ChIP-nexus experiment.

During the ChIP incubation, end repair and dA-tailing were performed using the NEBNext End Repair Module (NEB) and the NEBNext dA-Tailing Module (NEB). ChIP-nexus adaptors with mixed fixed barcodes (CTGA, TGAC, GACT, ACTG) were ligated with Quick T4 DNA ligase (NEB) and converted to blunt ends with Klenow fragment (NEB) and T4 DNA polymerase (NEB). The samples were treated with lambda exonuclease (NEB) and RecJf exonuclease (NEB) for generating Pol II footprints at high resolution. After each enzymatic reaction, the chromatin was washed with the nexus washing buffers A to D and Tris buffer (10 mM Tris, pH 7.5, 8.0, or 9.5, depending on the next enzymatic step). After RecJf exonuclease digestion, the chromatin was eluted and subjected to reverse crosslinking and ethanol precipitation. Purified single-stranded DNA was then circularized with CircLigase (Epicenter), annealed with oligonucleotides complementary to the BamHI restriction site and linearized by BamHI digestion. The linearized single-stranded DNA was purified by ethanol precipitation and subjected to PCR amplification with NEBNext High-Fidelity 2X PCR Master Mix (NEB) and ChIP-nexus primers. The ChIP-nexus libraries were then gel-purified before sequencing with Illumina NextSeq 500.

After sequencing, spiked-in samples were aligned to a dm6-hg38 combined genome. Only reads that uniquely aligned to each genome were used for analysis, and PCR duplicates with the same ChIP-nexus barcode were removed. Each *Drosophila* sample was then read-count normalized based on the ratio between human and *Drosophila* reads. Paused Pol II half-life calculation was performed on PRO-seq-validated promoters selected from 2023 non-overlapping genes separated from neighboring genes by at least 200 bp if a typical Pol II ChIP-nexus footprint was observed (distance between positive and negative strand peak < 50 bp, position of the Pol II footprint < 150 bp downstream of the TSS). 998 promoters fulfilled these criteria. For each promoter, the Pol II signal was calculated in a 51 bp window centered on the pausing position (the midpoint between Pol II positive and negative summits) and the Pol II time course measurements were fitted into an exponential decay model using non-linear regression. For display purposes (see heatmap in Figure 4C), the Pol II measurements at each promoter were normalized to the maximum Pol II signal in samples from cells not treated with triptolide.

QUANTIFICATION AND STATISTICAL ANALYSIS

Quantification of Western Blots

The intensities of bands corresponding to SSRP1, Spt16, and tubulin were measured using Image Studio Version 5.2.

Quantification of H3 ChIP-qPCR Assays

Enrichment as a percent of the input was calculated for each ChIP sample using the formula: $100^{*}\ 2^{\wedge}[Ct_{Input} - \log_2(800/30)\text{-}Ct_{IP}]$, where 800/30 is the input dilution factor. For each ChIP, H3 enrichments (ChIP/input) in promoter and gene body regions were normalized to the average of the ChIP/input values from two transcriptionally inactive genomic regions. In this experiment, Ct values of at least 2 technical replicates and 2 biological replicates were used for the analysis. Mean and standard deviation were calculated using Excel.

Statistical Analysis

Statistical analyses were performed using R and Bioconductor packages. Metagene plots and boxplots show the average values from replicates and were generated using ggplot2 (Wickham, 2009). P values were determined using the Wilcoxon rank sum test of pairwise comparisons. Differences were considered significant if P values were ≤ 0.05. In the figures, $p \leq 0.05$ is indicated by *; $p \leq 0.01$ by **; $p \leq 0.001$ by ***. Sample size (N) for each analysis is indicated in the figure legends.

DATA AND CODE AVAILABILITY

PRO-seq, RNA-seq, ChIP-seq and ChIP-nexus data have been deposited in NCBI's Gene Expression Omnibus (GEO) and are accessible through accession code GSE129236.

Original data underlying Figures 1A and S2 can be accessed from the Stowers Original Data Repository at https://www.stowers.org/research/publications/LIBPB-1282.